An automatic image processing algorithm for initiating and terminating intracoronary OFDI pullback

Lida P. Hariri,[1,2,*], Brett E. Bouma,[1,3,5] Sergio Waxman,[4] Milen Shishkov,[1,3] Benjamin J. Vakoc,[1,3,5] Melissa J. Suter,[1,3] Mark I. Freilich,[4] Wang-Yul Oh,[1,3] Mireille Rosenberg,[1] and Guillermo J. Tearney[1,2,5]

[1]*Wellman Center for Photomedicine, Massachusetts General Hospital, Boston, Massachusetts 02114 USA*
[2]*Department of Pathology, Massachusetts General Hospital, Boston, Massachusetts 02114 USA*
[3]*Department of Dermatology, Massachusetts General Hospital, Boston, Massachusetts 02114 USA*
[4]*Department of Cardiology, Lahey Clinic, Burlington, Massachusetts 01803 USA*
[5]*MIT-Harvard Division of Health Sciences and Technology, USA*
**lhariri@partners.org*

Abstract: Intracoronary optical frequency domain imaging (OFDI) provides high resolution, three-dimensional views of coronary artery microstructure, but requires a non-occlusive saline/contrast purge to displace blood for clear artery views. Recent studies utilized manual pullback initiation/termination based on real-time image observation. Automated pullback initiation/termination by real-time OFDI signal analysis would enable more efficient data acquisition. We evaluate the use of simple imaging parameters to automatically and robustly differentiate between diagnostic-quality clear artery wall (CAW) versus blood-obstructed fields (BOF). Algorithms are tested using intracoronary OCT human data retrospectively and intracoronary OFDI swine and human data prospectively. In prospective analysis of OFDI swine data, the sensitivity and specificity of the ratio of second and first moments (contrast parameter) were 99.6% and 97.2%, respectively. In prospective analysis of OFDI clinical data, the contrast parameter yielded 96.0% sensitivity and 94.5% specificity. Accuracy improved further by analyzing sequential frames. These results indicate the algorithm may be utilized with intracoronary OFDI for initiating and terminating automated pullback and digital data recording.

OCIS codes: (100.0100) Image processing; (100.2960) Image analysis; (110.4500) Optical coherence tomography; (110.0110) Imaging systems; (060.2350) Fiber optics imaging; (170.3880) Medical and biological imaging.

References and links

1. I. K. Jang, G. J. Tearney, B. MacNeill, M. Takano, F. Moselewski, N. Iftima, M. Shishkov, S. Houser, H. T. Aretz, E. F. Halpern, and B. E. Bouma, "In vivo characterization of coronary atherosclerotic plaque by use of optical coherence tomography," Circulation **111**(12), 1551–1555 (2005).
2. S. H. Yun, G. J. Tearney, B. J. Vakoc, M. Shishkov, W. Y. Oh, A. E. Desjardins, M. J. Suter, R. C. Chan, J. A. Evans, I. K. Jang, N. S. Nishioka, J. F. de Boer, and B. E. Bouma, "Comprehensive volumetric optical microscopy in vivo," Nat. Med. **12**(12), 1429–1433 (2007).
3. M. Kawasaki, B. E. Bouma, J. Bressner, S. L. Houser, S. K. Nadkarni, B. D. MacNeill, I. K. Jang, H. Fujiwara, and G. J. Tearney, "Diagnostic accuracy of optical coherence tomography and integrated backscatter intravascular ultrasound images for tissue characterization of human coronary plaques," J. Am. Coll. Cardiol. **48**(1), 81–88 (2006).
4. G. J. Tearney, I. K. Jang, and B. E. Bouma, "Optical coherence tomography for imaging the vulnerable plaque," J. Biomed. Opt. **11**(2), 021002 (2006).
5. D. Stamper, N. J. Weissman, and M. Brezinski, "Plaque characterization with optical coherence tomography," J. Am. Coll. Cardiol. **47**(8 Suppl), C69–C79 (2006).

#129489 - $15.00 USD Received 8 Jul 2010; revised 28 Jul 2010; accepted 8 Aug 2010; published 10 Aug 2010

6. M. E. Brezinski, "Optical coherence tomography for identifying unstable coronary plaque," Int. J. Cardiol. **107**(2), 154–165 (2006).
7. T. Kubo, T. Imanishi, S. Takarada, A. Kuroi, S. Ueno, T. Yamano, T. Tanimoto, Y. Matsuo, T. Masho, H. Kitabata, K. Tsuda, Y. Tomobuchi, and T. Akasaka, "Assessment of culprit lesion morphology in acute myocardial infarction: ability of optical coherence tomography compared with intravascular ultrasound and coronary angioscopy," J. Am. Coll. Cardiol. **50**(10), 933–939 (2007).
8. S. Chia, O. Christopher Raffel, M. Takano, G. J. Tearney, B. E. Bouma, and I. K. Jang, "In-vivo comparison of coronary plaque characteristics using optical coherence tomography in women vs. men with acute coronary syndrome," Coron. Artery Dis. **18**(6), 423–427 (2007).
9. M. E. Brezinski, "Applications of optical coherence tomography to cardiac and musculoskeletal diseases: bench to bedside?" J. Biomed. Opt. **12**(5), 051705 (2007).
10. M. Takano, I. K. Jang, S. Inami, M. Yamamoto, D. Murakami, K. Okamatsu, K. Seimiya, T. Ohba, and K. Mizuno, "In vivo comparison of optical coherence tomography and angioscopy for the evaluation of coronary plaque characteristics," Am. J. Cardiol. **101**(4), 471–476 (2008).
11. G. J. Tearney, S. Waxman, M. Shishkov, B. J. Vakoc, M. J. Suter, M. I. Freilich, A. E. Desjardins, W. Y. Oh, L. A. Bartlett, M. Rosenberg, and B. E. Bouma, "Three-dimensional coronary artery microscopy by intracoronary optical frequency domain imaging," JACC Cardiovasc. Imaging **1**(6), 752–761 (2008).
12. G. van Soest, T. Goderie, E. Regar, S. Koljenović, G. L. van Leenders, N. Gonzalo, S. van Noorden, T. Okamura, B. E. Bouma, G. J. Tearney, J. W. Oosterhuis, P. W. Serruys, and A. F. van der Steen, "Atherosclerotic tissue characterization in vivo by optical coherence tomography attenuation imaging," J. Biomed. Opt. **15**(1), 011105 (2010).
13. P. Barlis, N. Gonzalo, C. Di Mario, F. Prati, L. Buellesfeld, J. Rieber, M. C. Dalby, G. Ferrante, M. Cera, E. Grube, P. W. Serruys, and E. Regar, "A multicentre evaluation of the safety of intracoronary optical coherence tomography," EuroIntervention **5**(1), 90–95 (2009).
14. P. Barlis, and J. M. Schmitt, "Current and future developments in intracoronary optical coherence tomography imaging," EuroIntervention **4**(4), 529–533 (2009).
15. A. F. Low, Y. Kawase, Y. H. Chan, G. J. Tearney, B. E. Bouma, and I. K. Jang, "In vivo characterisation of coronary plaques with conventional grey-scale intravascular ultrasound: correlation with optical coherence tomography," EuroIntervention **4**(5), 626–632 (2009).
16. P. Barlis, G. van Soest, P. W. Serruys, and E. Regar, "Intracoronary optical coherence tomography and the evaluation of stents," Expert Rev. Med. Devices **6**(2), 157–167 (2009).
17. F. Prati, E. Regar, G. S. Mintz, E. Arbustini, C. Di Mario, I. K. Jang, T. Akasaka, M. Costa, G. Guagliumi, E. Grube, Y. Ozaki, F. Pinto, and P. W. Serruys, "Expert review document on methodology, terminology, and clinical applications of optical coherence tomography: physical principles, methodology of image acquisition, and clinical application for assessment of coronary arteries and atherosclerosis," Eur. Heart J. **31**(4), 401–415 (2010).
18. B. D. MacNeill, H. C. Lowe, M. Takano, V. Fuster, and I. K. Jang, "Intravascular modalities for detection of vulnerable plaque: current status," Arterioscler. Thromb. Vasc. Biol. **23**(8), 1333–1342 (2003).
19. B. D. MacNeill, B. E. Bouma, H. Yabushita, I. K. Jang, and G. J. Tearney, "Intravascular optical coherence tomography: cellular imaging," J. Nucl. Cardiol. **12**(4), 460–465 (2005).

1. Introduction

Intracoronary optical coherence tomography (OCT) is currently the preferred technique for imaging human coronary arteries at the level of detail required for identifying microscopic features associated with high-risk plaques and for measuring tissue overlying stent struts [1–19]. The first generation of catheter-based time-domain OCT (TD-OCT) imaging of coronary arteries necessitated the use of long saline purges or balloon occlusion to clear blood from the field of view. While a substantial amount of imaging data was acquired using these methods of blood removal for TD-OCT [1,3–10,12–19], these techniques were cumbersome clinically and limited the amount of data that could be acquired from coronary arteries *in vivo*. A new generation of OCT, termed optical frequency domain imaging (OFDI, also known as frequency-domain OCT (FD-OCT)), obtains images 10-100 times faster than the earlier generation technique at a resolution less than 10 μm [2,11]. This high imaging speed allows for three-dimensional, high resolution imaging of coronary artery segments and specifically addresses the blood contamination problem by enabling the screening of an entire coronary artery following a brief, non-occlusive saline purge and rapid pullback of the catheter optics [11].

#129489 - $15.00 USD Received 8 Jul 2010; revised 28 Jul 2010; accepted 8 Aug 2010; published 10 Aug 2010

At present, our OFDI system initiates the pullback (and also the data recording) manually by an operator who pushes a button when the real-time image display shows an arterial wall that is unobstructed by blood. The pullback is manually terminated when blood re-enters the image field or when an image of the guide catheter is observed. With our system, data recording only occurs when the pullback is active, thereby minimizing the stored data size [2,4,8,11]. While this method appears to work effectively, an automated method for initiating and terminating pullback is more desirable, as it could reduce collection and storage of unusable blood contaminated data, simplify the imaging procedure, and diminish the possibility of human error. There are commercially available intravascular OCT devices which provide automatic catheter pullback based on saline injection timing [17]. In the early stages of the development of the OFDI system, we considered using a signal from the saline injector to initiate and terminate pullback and digital recording. This approach was complicated, however, by the variability of the time delay between initiation of the injection and the onset of clear imaging, which depends upon factors such as placement of the guide catheter within the vessel ostium and the presence and location of stenoses within the vessel.

An alternative approach is to obtain a control signal for pullback and data archiving by conducting signal/image analysis on the OFDI image data in real time. In order to determine whether or not the control signal should be set, the algorithm will need to distinguish diagnostic quality images of artery wall from blood-obstructed field or guide catheter. This control signal would be set and pullback/digital storage would occur only when OFDI image frames contained diagnostic quality images of artery wall. Advantages to this automatic process includes simplification of the imaging procedure and the possibility of optimizing pullback and storage when the saline purge is variably effective, such as that which might occur during a manual flush. In this study, we have developed and validated algorithms to differentiate diagnostic quality OCT/OFDI images of artery wall from images of blood-obstructed field and guide catheter.

2. Materials and methods

2.1. Overview

Three studies were conducted to classify individual OCT/OFDI image frames as either (1) diagnostic quality images of artery wall versus blood-obstructed fields and (2) guide catheter or non-guide catheter. Algorithms were tested using three de-identified data sets: (1) Intracoronary OCT human data obtained from a previously conducted clinical study with a first generation OCT system/catheter [1], (2) Intracoronary OFDI data obtained from swine [2], and (3) Intracoronary OFDI data obtained from human subjects in an ongoing clinical study [11]. The algorithms were tested retrospectively with the OCT data and prospectively with the OFDI data. OCT/OFDI images were interpreted by an expert reader (G.J.T.) and classified into four categories: (1) clear artery wall (CAW), (2) blood/wall mixture (BWM), (3) blood obstructed field (BOF), and (4) guide catheter (GC) (Fig. 1). Sensitivities, specificities, and/or error rates were computed using the expert reader determination as the gold standard.

Parameters were computed on log10-demodulated data in polar coordinates (prior to circularization). Prior to analysis, images were histogram equalized to a rectangular (uniform) probability distribution function.

#129489 - $15.00 USD Received 8 Jul 2010; revised 28 Jul 2010; accepted 8 Aug 2010; published 10 Aug 2010

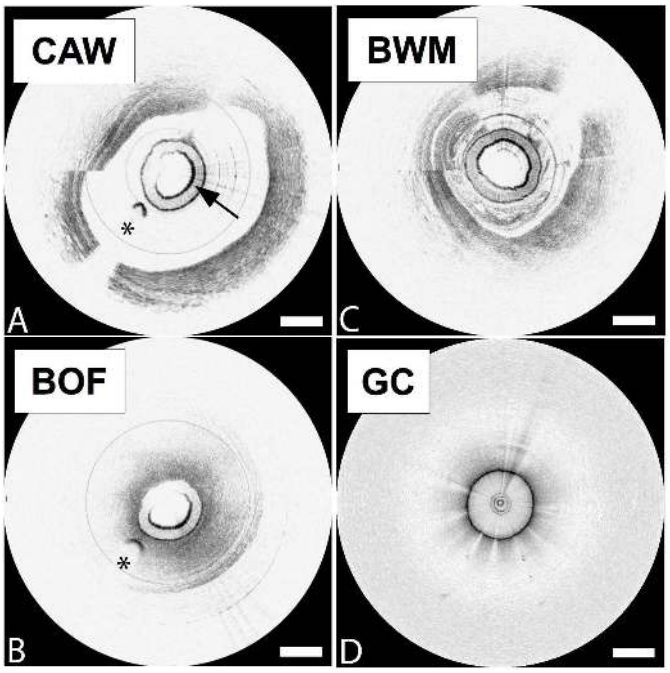

Fig. 1. Intracoronary OCT images from human coronary artery and their classifications. A. Clear artery wall. The catheter sheath is denoted by an arrow. B. Blood obstructed field. C. Blood-wall mixing. D. Guide catheter. Images are displayed with an inverse gray scale LUT. The asterisk ("*") denotes the guide wire artifact. Scale bar, 500 µm.

2.2. Diagnostic-quality images of artery wall versus blood obstructed field

A number of intensity metrics for identifying clear, diagnostic-quality images were evaluated, including the first, second, and third order moments and contrast parameter (CP), defined as the second order moment over the first order moment [Eq. (1)]:

$$CP = \frac{StDev(AlineROI)}{Mean(AlineROI)} = \frac{SecondMoment}{FirstMoment} \tag{1}$$

After assessment of the different metrics, we determined that the contrast parameter provided the most promise for achieving the highest accuracy for classification of CAW. A small training data set was used to determine the CP threshold. The contrast parameter was computed on either a per A-line or every 5th A-line basis (over a 33-pixel or 340 µm 1D-ROI starting at the outer sheath reflection, Fig. 2) in each 500 A-line image. Within a single image, the number of contrast parameters calculated for each A-line that exceeded a threshold was computed. If the fraction of A-lines classified as artery was greater than or equal to 0.36 per image, the entire image was classified as CAW. The fraction of A-lines was set to 0.36 because the guide wire typically obscured 15-20% of each image, and as a result, a fractional value of 0.36 equated to approximately half of the image. If the fraction of A-lines classified as artery was less than 0.36 per image, the entire image was classified as BOF. The accuracy of the contrast parameter was tested retrospectively on the OCT clinical data set and prospectively on the OFDI swine and human data, after adjustment of the thresholds which were determined using a small training data set. All computations were performed in Matlab 2007b (MathWorks, Natick, Massachusetts) on a MacBook laptop using MAC OS X operating system, version 10.4.11, with a 2 GHz Intel Core 2 Duo processor, 117 GB hard drive, and 2 GB, 667 MHz DDR2 RAM.

#129489 - $15.00 USD Received 8 Jul 2010; revised 28 Jul 2010; accepted 8 Aug 2010; published 10 Aug 2010

2.3. Presence or absence of guide catheter

Following the evaluation of the different metrics above, we determined that the second moment provided the best determination of the absence or presence of guide catheter. To determine whether or not the image should be classified as GC, the intensity second moment was computed over a 500 (x) x 150 (z) (4.5 x 1.35 mm) 2DROI that started outside the outer sheath (Fig. 2). The second moment for each image was then compared to a threshold. Only the OFDI swine data was used for this experiment. A small training set was used to determine the threshold and the remainder of the data was used for prospective determination of the accuracy for GC classification.

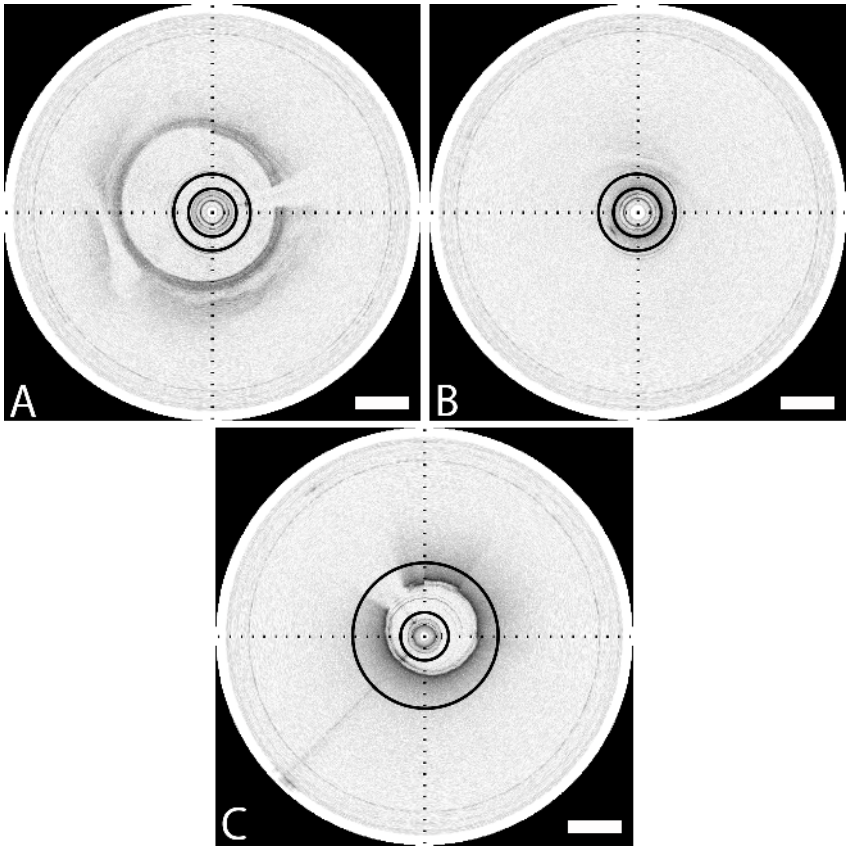

Fig. 2. Intracoronary OFDI in swine demonstrating algorithm ROI. (a) CP algorithm 33 pixel 1D ROI calculated every A-line or every 5th A-line in clear artery wall and (b) blood obstructed field. (c) Standard deviation algorithm 150 pixel 2D ROI in guide catheter image. Black circles bound ROI for each respective algorithm. Images are displayed with an inverse gray scale LUT. Scale bar, 500 μm.

3. Results

3.1. OCT and OFDI interpretation by expert reader

The intracoronary OCT human images were obtained from 82 patients. Images were classified as CAW (n = 253 images), BOF (n = 220), and BWM (minor contamination of field with blood, with diagnostic-quality artery wall images, n = 118).

#129489 - $15.00 USD Received 8 Jul 2010; revised 28 Jul 2010; accepted 8 Aug 2010; published 10 Aug 2010

The intracoronary OFDI swine data was obtained from 13 living swine. Images were classified as CAW (n = 4444 images), BOF (n = 1176), or BWM (n = 1341). A total of n = 962 images were classified as GC and n = 6961 were non-GC.

Intracoronary OFDI human data was obtained from 11 patients. As the algorithm is binary, assigning images as either clear artery wall or blood obstructed field for catheter pullback initiation or termination, respectively, the images in this analysis were similarly classified as either CAW (including BWM images, n = 2841 images) and BOF (n = 1468). Data analyzed every 5th A-line was computed at 20 frames/second for all OCT and OFDI data.

3.2. Diagnostic-quality images of artery wall versus blood obstructed field

3.2.1. Intracoronary OCT human data

The contrast parameter demonstrated a sensitivity of 99.2% and 91.5% for CAW and BWM, respectively, and a specificity of 96.4% (where CP ≥ 0.34 classifies an A-line as artery and an artery image is defined as ≥ 36% of A-lines in an image classified as artery). Comparable sensitivities and specificities were obtained with contrast parameter thresholds ranging from 0.3 to 0.4.

We also investigated the possibility of using fewer A-lines per image, in order to decrease computation time. The contrast parameter was evaluated using every 5th A-line as opposed to every A-line. With this analysis, sensitivities for CAW and BWM were 98.4% and 90.7%, respectively, and the specificity was 95.0%.

3.2.2. *Intracoronary OFDI swine data*

Once the algorithm was developed using the OCT clinical data, it was then applied prospectively to OFDI data obtained from the coronary arteries of living swine. Because the clinical OCT data set was obtained from human rather than swine data and the images were acquired with a different imaging system/catheter, the contrast parameter cut-off was re-evaluated for the swine data set. A small training set of 500 images (CAW: n = 347, BWM: n = 64, BOF: n = 12, GC: n = 77) from 1 pig was used to determine the appropriate contrast parameter cutoff. Analysis of this training set demonstrated good results when the contrast parameter threshold to classify an A-line as artery was ≥ 0.1. Using this cutoff applied prospectively to the remainder of the OFDI swine data, the sensitivities were 99.6% (95% CI: 99.4-99.8%) and 99.3% (95% CI: 98.9-99.7%) for CAW and BWM, respectively, and the specificity was 97.2% (95% CI: 96.3-98.1%) when calculated for every 5th A-line in each image. The analysis was re-evaluated with additional criterion that ≥ 3 consecutive images must be classified in the same category before a transition from one state to another was determined. This approach resulted in sensitivities of 99.8% (95% CI: 99.7-99.9%) and 100% for CAW and BWM, respectively, and a specificity of 97.6% (95% CI: 96.7-98.5%). Error rates were also calculated, including early termination, late termination, early trigger, late trigger, and total error rate for data calculated every 5th A-line with the additional criterion that ≥ 3 consecutive images must be classified in the same category before a transition was recognized (Table 1).

3.2.3. Intracoronary OFDI human data

The contrast parameter cut-off was re-evaluated for the OFDI clinical data using a small training set of 465 images (CAW: n = 266, BOF: n = 199) from 1 patient. Analysis of this training set demonstrated the optimal results when the contrast parameter threshold to classify an A-line as artery was ≥ 0.35. This cut-off was applied prospectively to the remaining OFDI clinical data, yielding a 96.0% sensitivity (95% CI: 95.2-96.7%) and a 94.1% specificity (95% CI: 92.8-95.3%) when calculated for every A-line in each image. Similar results were obtained when the analysis was completed computing CP on every 5th A-line, with 96.0% sensitivity

#129489 - $15.00 USD Received 8 Jul 2010; revised 28 Jul 2010; accepted 8 Aug 2010; published 10 Aug 2010

(95% CI: 95.1-96.6%) and 94.5% specificity (95% CI: 94.1-95.6%). The analysis was re-evaluated with additional criterion that ≥ 3 consecutive images must be classified in the same category before a transition from one state to another was recognized. This approach resulted in 95.9% sensitivity (95% CI: 94.7-96.8%) and 96.2% specificity (95% CI: 95.4-96.9%) when calculated for every 5th A-line in each image. Error rates were also calculated, including early termination, late termination, early trigger, late trigger, and total error rate for data calculated every 5th A-line with the additional criterion that ≥ 3 consecutive images must be classified in the same category before a transition was recognized (Table 1).

3.3. Presence or absence of guide catheter: intracoronary OFDI swine data

Using the OFDI swine training set described above (GC: n = 77, non-GC: n = 423), a second moment threshold of ≥ 44.5 was selected to classify an image as GC. When tested on the remaining OFDI swine images, the sensitivity and specificity of the second moment for guide catheter classification were 98.1% (95% CI: 97.2-99.0%) and 99.8% (95% CI: 99.7-99.9%), respectively. The analysis was re-evaluated with the additional criterion that ≥ 3 consecutive images must be classified in the same category before a transition was recognized, resulting in 100% sensitivity and specificity for guide catheter classification.

Table 1. Error Rates for OFDI Swine and Clinical Data

	Early Termination	Late Termination	Early Trigger	Late Trigger	Total Error Rate
OFDI Swine Data	0.13%	0.26%	0.23%	0%	0.62%
OFDI Clinical Data	2.2%	0.4%	1.4%	0%	4.0%

4. Discussion

Our results show that simple image processing techniques can be utilized to determine 1) when the OFDI image contains a clear, diagnostic-quality view of the artery wall, as opposed to a blood obstructed view and 2) when the image contains guide catheter. These parameters were computed at 20 frames/second in Matlab 2007b on a standard MacBook laptop. Computation time could be improved by using more rapid programming languages (such as C or C + +), libraries such as the Intel Performance Primitives (IPP) on a personal computer, or dedicated digital signal processing, such as field-programmable gate arrays. In turn, the algorithms may be utilized to generate a control signal in real-time to start and stop pullback and digital data recording (Fig. 3).

The results were very encouraging, demonstrating sensitivities and specificities > ~98% for the OFDI swine data and > ~95% for the OFDI clinical data. The consistency of the CP cut-off among OCT and OFDI clinical data demonstrates that the threshold parameters may be fairly constant between difference imaging systems. Comparable sensitivities and specificities with ranging CP thresholds in the OCT clinical data support the algorithm robustness.

Intracoronary OFDI typically includes imaging of atherosclerotic lesions and/or stented vessels. It is imperative that the algorithms perform equally well in these scenarios. The OCT and OFDI clinical data sets included both atherosclerotic plaques and stented vessels, neither of which affected algorithm performance.

Further improvement in performance can be anticipated by simple modifications of the algorithm. The initial analyses conducted in this study were developed and tested on a per-image basis. We have noticed, however, that when misclassifications occurred, they tended to be isolated and not repeated over several frames. By placing an additional constraint on the classification, such as presence of a classification for more than 3 consecutive frames, our accuracy was found to improve to >~95% for OFDI clinical data and >~98% for OFDI swine data.

#129489 - $15.00 USD Received 8 Jul 2010; revised 28 Jul 2010; accepted 8 Aug 2010; published 10 Aug 2010

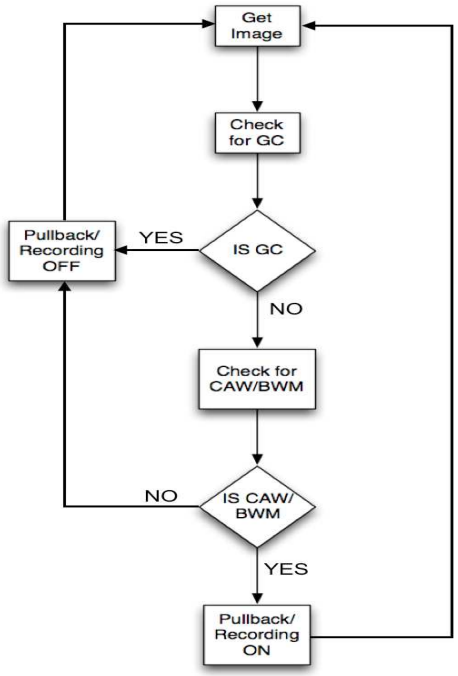

Fig. 3. Flow diagram for OFDI pullback storage image feedback and control.

One potential limitation to the use of these algorithms is that the selection of the appropriate ROI requires that the location of outer catheter sheath is known. Normally, prior to data acquisition, the location of the outer sheath is set to reside at a certain pixel location in the image. However, during the imaging procedure, small variations in the location of the sheath can occur which may affect the accuracy of the algorithms. Future work will be directed at evaluating the robustness of the algorithms given these potential variations in outer sheath location. If required, additional automatic computational methods will need to be developed to determine the sheath location in real time. In this study, we have developed and validated algorithms to differentiate diagnostic quality OCT/OFDI images of artery wall from images of blood-obstructed field and guide catheter. We have determined that the contrast parameter calculated over a 33 pixel 1D ROI (outside the catheter sheath reflection) was the best parameter for differentiating CAW from BOF. The performance of this parameter was similar whether calculated every A-line or every 5th A-line, thus allowing for decreased computation time. The standard deviation calculated over a 150 pixel 2D ROI was the best parameter for distinguishing GC from non-GC. Both parameters performed best with the additional criterion that ≥ 3 consecutive images must be classified in the same category before a transition was recognized.

Acknowledgments

This work was supported in part by the National Institutes of Health under Grant R01HL076398 (NHLBI). Terumo Corporation sponsors non-clinical OFDI research in the laboratory of Drs. Tearney and Bouma and has a technology-licensing arrangement with Massachusetts General Hospital. Drs. Tearney and Bouma have the right to receive licensing income from Terumo Corporation.

#129489 - $15.00 USD Received 8 Jul 2010; revised 28 Jul 2010; accepted 8 Aug 2010; published 10 Aug 2010